2026 IEEE International Conference on Robotics and Automation (ICRA 2026)
June 1-5, 2026. Vienna, Austria

Variable Stiffness Soft Robotic Arm with Positive-Pressure Layer Jamming for Enhanced Load Capacity

Zekai Wu[1,2],Xin Fu[1,2],Daohui Zhang[1] and Xingang Zhao[1]

Abstract— **Soft robotic arms have attracted considerable attention in high-interaction scenarios owing to their intrinsic safety and adaptability. Nevertheless, their application is often limited by low load capacity. To address this issue, this paper introduces a layered jamming variable stiffness mechanism applicable to corrugated spring shell structures, which typically possess high torsional stiffness but inadequate tensile and bending rigidity. The proposed design integrates an internal airbag and a jamming plate interlayer within an external corrugated spring structure. By controlling the air pressure inside the bag, the normal pressure applied to the jamming layers can be precisely regulated, thereby enabling dynamic adjustment of the overall structural stiffness. Experimental results demonstrate that under an air pressure of 30 kPa, a six-layer jamming plate configuration achieves a tensile stiffness of approximately 100 N/mm and supports tensile loads exceeding 500 N. These values represent a 70-fold improvement in stiffness and a 20-fold increase in load capacity compared to the non-reinforced structure. Additionally, the system retains omnidirectional bending capability via tendon-driven actuation, with a maximum bending angle of 40° per segment. Multiple units can be serially connected to form a manipulator with an extended workspace. This study highlights the efficacy of the layered jamming mechanism in significantly enhancing the stiffness and load-bearing performance of flexible robotic arms, providing a viable solution for applications requiring both compliance and strength.**

I. INTRODUCTION

Soft robots offer notable advantages over traditional rigid robots in human-robot interaction scenarios, owing to their inherent compliance and adaptability. However, their typically low-modulus material composition also results in limited load-bearing capacity. In response, numerous studies have focused on enhancing the stiffness of soft robots to improve their performance under external loads. Existing approaches can be broadly categorized into two types: rigid-flexible coupling design and variable stiffness mechanisms.

Rigid-flexible coupling strategies frequently utilize internal skeletal reinforcement to provide structural support [1], [2]. Alternatively, reinforcement methods analogous to exoskeletons are also employed to enhance structural performance [3]. While this method yields high stability, it lacks the capability for active stiffness adjustment during operation and depends heavily on pre-determined structural parameters. In contrast, variable stiffness designs enable dynamic control over mechanical properties. Commonly adopted methods include layer jamming, antagonistic actuation, and the use of phase-change materials[4], [5]. These techniques allow real-time modulation of robotic stiffness, enhancing adaptability across various task requirements. The antagonistic variable stiffness scheme represents a significant exploration of biomimicry inspired by human musculoskeletal systems. In recent years, researchers have developed various methods to realize antagonistic variable stiffness. These approaches include mechanisms based on body-tendon antagonism [6], [7], spring-based opposition [8], [9], fluid-driven versus tendon-driven actuation [10], [11], and mutual opposition between fluid-driven units [6], [12], [13]. The layer jamming technique is widely employed in soft robotics due to its compact form factor, wide stiffness variability, and adaptability to diverse deformations. Based on the filler material used, it can be categorized into particle jamming [14], fiber jamming [15], [16], [17], [18], [19], and layer jamming.

Kim et al. [20] first introduced the concept of layer jamming in 2013, utilizing a threaded connection ring and a thin-film seal to enable interlayer adhesion and enhanced friction under negative pressure. Subsequent studies have since improved, optimized, and applied this structure in various contexts [21], [22], [23], [24], [25], though the underlying mechanism remains dependent on vacuum-induced interlayer bonding, which imposes stringent sealing requirements. Alternative approaches have also been developed to overcome this limitation. J.L.C. Santiago et al. [26] proposed an external spring compression mechanism for layer confinement in 2016. T. Wang et al. [27] introduced an electrostatic layer jamming method in 2019, leveraging electrostatic attraction to clamp and jam material layers. More recently, P. Li et al. [28] presented a positive-pressure layer jamming strategy for growing robots in 2025, which achieves stiffness through the compression of jamming layers against an external constraint via an internal expanding body. These innovations demonstrate how fundamental principles can be adapted to simplify structures and broaden application scenarios.

The corrugated spring structure is a damping element adapted from conventional manufacturing processes. E. H. Skorina and C. D. Onal [29] employed 3D-printed soft materials to enhance the torsional stiffness of soft robots, demonstrating significant performance improvements. J. M. Salgueiro and J. C. P. Reis [30] utilized corrugated spring structures directly as the robotic body, leveraging their inher-

*This work was supported in part by the National Key Research and Development Program of China (2023YFB4704700, 2023YFB4704702, 2022YFF1202500, 2022YFF1202502) and the National Natural Science Foundation of China (62273336, 92048302, 92048203, U20A20197, U22A2067).

[1]State Key Laboratory of Robotics and Intelligent Systems, Shenyang Institute of Automation, Chinese Academy of Sciences, Shenyang, China.
[2]University of Chinese Academy of Sciences, Beijing, China.
∗Contact: Daohui Zhang (zhangdaohui@sia.cn)

ent elasticity for passive self-recovery and achieving multi-modal deformation via tendon-driven actuation. This type of structure offers a wide range of potential stiffness values depending on manufacturing parameters such as geometry and material properties. However, since the stiffness is predetermined by these structural design choices, it cannot be adjusted during task execution, limiting its adaptability in dynamic environments.

The primary contribution of this work is the design of a positive-pressure layered jamming mechanism applicable to continuum robots, which significantly enhances structural rigidity and load-bearing capacity while preserving full omnidirectional bending capability. Leveraging this principle, we have constructed a robotic system consisting of multiple variable-stiffness modules, which can be connected in series to accommodate varying operational length requirements. Each module utilizes a corrugated spring exterior housing an internal airbag and jamming layers, enabling wide-range modulation of both stiffness and load capacity. Tendons anchored to the shell provide active omnidirectional actuation for bending, and the jamming mechanism allows pneumatic expansion during curvature to achieve load-resistant self-locking.

The remainder of this paper is organized as follows: Section II details the working principle, structural design, fabrication, and assembly process of the proposed system, and introduces the load model and performance metrics. Section III presents a parametric analysis of the variable stiffness components, along with experimental validations including bending and load tests on a single segment, as well as motion and load-bearing evaluations of a multi-segment assembly. The final section summarizes the main conclusions and outlines directions for future research.

II. DESIGN AND MANUFACTURING

A. Structural Principle Description

The design draws inspiration from a well-known phenomenon: when two books are stacked and their pages interleaved, pulling them apart requires significant force due to friction between the pages under self-weight. In this mechanism, the separation force can be modulated by varying both the number of overlapping layers and the applied normal pressure. We simplified and adapted this principle by integrating a stack of interleaved layers within a corrugated spring housing. The bending and extension of the spring are analogous to the sliding of book pages, while the adjustable pressure enables customized control over the separation force—and thus the overall stiffness. Note that compression stiffness, which involves antagonistic regulation via airbag and tendon actuation, falls outside the scope of this study.

B. Structure Design and Materials

To achieve continuous stiffness control in the system, we designed a positive pressure pneumatic layer jamming mechanism. The tested structural unit has an original length of 120 mm and a diameter of 52 mm. The overall and detailed assembly are illustrated in Fig. 1 (a) and (b). The structure consists of a corrugated spring shell, a limiting layer, a jamming layer, an internal airbag, and end covers. The corrugated spring is fabricated from nylon via SLS(Selective Laser Sintering), with three circumferentially distributed tendon routing holes for actuation. Thickened protrusions on both ends facilitate connection to the end covers, jamming layer, and limiting layer. The limiting layer is made of stretchable fabric, tailored to size and placed between the spring and the jamming layer. For clarity in structural visualization, this layer is omitted in certain diagrams. The jamming layer comprises multiple jamming plates made by PLA(Poly Lactic Acid), each with a thickness of 0.2 mm. Each plate features four holes: two for mounting to the end cover and two for interlocking with the corrugated spring. This design significantly simplifies the assembly process.The jamming plate is designed with a bifurcated shape to accommodate structural bending. This design ensures that, at any bending angle, at least a subset of the jamming layers remains under tension and separated, thereby maximizing the jamming effect and enhancing overall structural stiffness. The airbag is a cylindrical silicone component fabricated through casting. Two types of end covers are used, both 3D-printed in PLA: a connecting end cover for joining multiple variable stiffness units, and an encapsulating end cover used at the terminal end of the structure. The latter includes dedicated holes for easy and rapid integration with various actuators, thereby extending the functional applicability of the system.

C. Fabrication and Assembly Process

The majority of structural components are fabricated using additive manufacturing techniques. The corrugated springs are produced in nylon via SLS, while the end caps and jamming plates are printed in PLA using fused deposition modeling (FDM). The silicone airbag is cast using a custom mold, which is also FDM-printed, as depicted in Fig. 1. The airbag is manufactured in three parts: a main body and two side covers. These components are bonded using a silicone-specific adhesive (JVKAN 988A, Special Silicone Adhesive) and subjected to an airtightness test prior to final assembly.

The narrow interlayer gaps and high number of layers in the jamming structure make direct assembly challenging and susceptible to misalignment. To address this, a dedicated assembly process has been developed to optimize manufacturing accuracy and reliability. As illustrated in Fig. 1 (c), the stacking method and interlayer bonding of the single-sided jamming plates are clearly defined. Fig. 1 (d) demonstrates the assembly sequence of the core structure, which is composed—from outer to inner—of the limiting layer, the jamming layer, and the end cover. The assembly procedure is as follows: first, the limiting layer is placed over the jamming plate; next, a bolt is inserted to secure the layer to the end cover; the airbag is then inserted into the resulting sub-assembly. Finally, the entire core structure is installed into the corrugated spring housing.

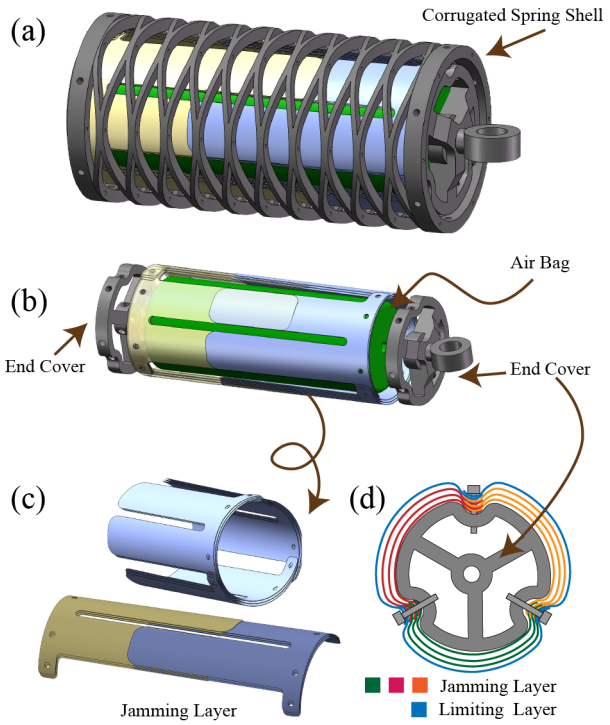

Fig. 1. Overall Structure and Assembly Details. (a) Complete variable stiffness structure. (b) Exploded view of the unit. (c) Jamming plates stacking and assembly method. (d) Interlayer configuration and end-cover connection.

D. Load Model

The load-bearing capacity of the structure is characterized by two key properties: the stiffness $K = dF/dx$ and the maximum load-bearing capacity $F_{\max}$.

Fig. 2 depicts the simplified mechanical model of the structure. In this representation, the non-overlapping and overlapping regions of the interference plates on both sides are assumed to exhibit distinct stiffness characteristics and are arranged in a series configuration.

The load-bearing capacity of the structure consists of two components: the intrinsic capacity provided by the outer corrugated spring shell and the internal airbag, and the additional capacity provided by the jamming layers and airbag expansion after inflation. The intrinsic load-bearing capacity can be expressed as (1):

$$F_{\text{elastic}}(x) = k_0 x + \int_0^x k_{\text{air}}(\xi)\, d\xi \tag{1}$$

where k_{air} is the equivalent tensile stiffness of the airbag, and k_0 is the stiffness of the outer corrugated spring shell. Simultaneously, due to the internal pressure acting on the axial end-face, the end-face experiences a pushing force:

$$P_{\text{push}} = PA_{\text{eff}} \tag{2}$$

where A_{eff} is the cross-sectional area of the airbag internal cavity.

The radial expansion of the airbag exerts pressure on the jamming plates. The maximum static friction between the jamming layers is given by:

$$F_{\max}(x) = 6(2n-1)\mu_s PA_0 \left(1 - \frac{x_p}{x_{\max}}\right) \tag{3}$$

When the total external tensile force satisfies the condition:

$$F > F_{\text{total}}(x) = F_{\text{elastic}}(x) + F_{\text{jam}}(x, x_p) \tag{4}$$

interlayer sliding occurs within the structure, and the friction transitions into interlayer kinetic friction, expressed as:

$$F_{\text{kin}}(x) = 6(2n-1)\mu_k PA_0 \left(1 - \frac{x}{x_{\max}}\right) \tag{5}$$

where μ_s is the coefficient of static friction, μ_k is the coefficient of kinetic friction, and x_p is the cumulative slip distance of the jamming layer. F_{jam} is defined as follows, where k_1 and k_2 are shown in Fig. 2:

$$F_{\text{jam}}(x, x_p) = \begin{cases} K_{\text{jam}}(x - x_p), & \text{if } K_{\text{jam}}(x - x_p) < F_{\max}(x) \\ F_{\text{kin}}(x), & \text{if } K_{\text{jam}}(x - x_p) \geq F_{\max}(x) \end{cases} \tag{6}$$

$$K_{\text{jam}} = \left(\frac{1}{k_1} + \frac{1}{k_2} + \frac{1}{k_1}\right)^{-1} \tag{7}$$

Following significant sliding, the overlapping area of the jamming layers decreases, causing the total tensile force to fall below the static friction threshold. Consequently, the structure relocks and enters the next cycle, resulting in the stick-slip effect.

Therefore, the equivalent tangent stiffness of the structure is:

$$K_{\text{macro}} = \frac{\partial F_{\text{macro}}}{\partial x} = k_0 + k_{\text{air}} + \frac{6(2n-1)\mu_k PA_0}{x_{\max}} \tag{8}$$

This stiffness characterizes the overall trend and is primarily composed of two parts: the structural stiffness of the body and the frictional softening caused by structural disengagement. When the air pressure P is low and the number of layers n is small, the first term dominates, $K_{\text{macro}} > 0$, and the curve shows an upward trend. When the two terms cancel each other out, $K_{\text{macro}} \approx 0$, leading to a flat plateau. When P is high and n is large, the initial friction is substantial, and the loss of friction upon sliding is severe (dominated by the second term), resulting in $K_{\text{macro}} < 0$, where the curve shows a downward trend. The subsequent experimental results also follow this pattern to a certain extent.

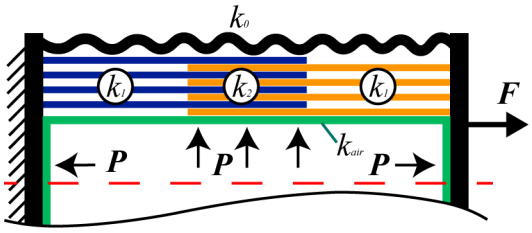

Fig. 2. Schematic diagram of the simplified structural model for stiffness analysis.

III. EXPERIMENTS AND RESULTS

In this section, we begin by introducing the experimental setup and test structure. Subsequently, comparative tests are carried out on components that may influence load capacity. The bending resistance of individual units is then evaluated. Finally, partial suspended-load comparative tests are conducted using a two-unit serial configuration as a robotic arm prototype.

A. Test Setup and Experiment Procedure

As illustrated in Fig. 3.(a), the stiffness of the structure is evaluated using a tensile testing system equipped with a 500 kg load cell (Transcell, BSS-500 kg, 120 Hz). The custom-designed end fixture allows the unit to be securely mounted to the tester, ensuring accurate and repeatable measurements.

The tensile test was conducted at a displacement rate of 20 mm/min across a 20 mm travel distance to minimize dynamic artifacts and ensure data stability. As shown in Fig. 3(b), compressed air was supplied by an oil-free silent air compressor (ZHIPU Silence Oil Free Air Compressor) and regulated through a precision pressure-reducing valve (SMC, IR2000, range: 0.01–0.2 MPa) before being delivered to the internal airbag. This configuration provided accurate and consistent pressure control during all experimental procedures.

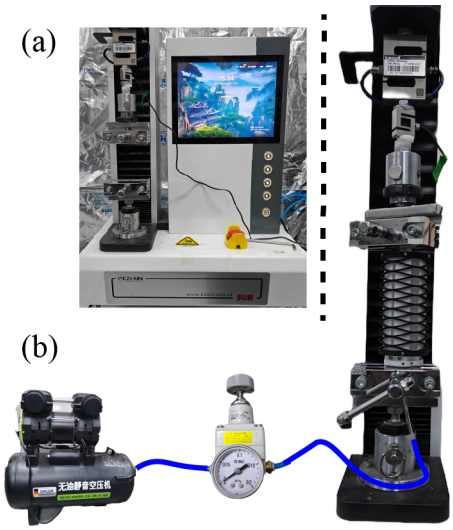

Fig. 3. (a) Tensile testing system. (b) Schematic diagram of the overall tensile test setup.

B. Influence of Internal Structure on Unit Stiffness

The normal force between the jamming plates is generated by the expansion of the internal airbag. In the uninflated state, the airbag has a small diameter and remains detached from the plates. The deformation behavior of the airbag upon inflation thus significantly influences the structural stiffness modulation capability. To investigate the effect of airbag material stiffness on system performance, three silicone materials with different Shore hardness values were tested:

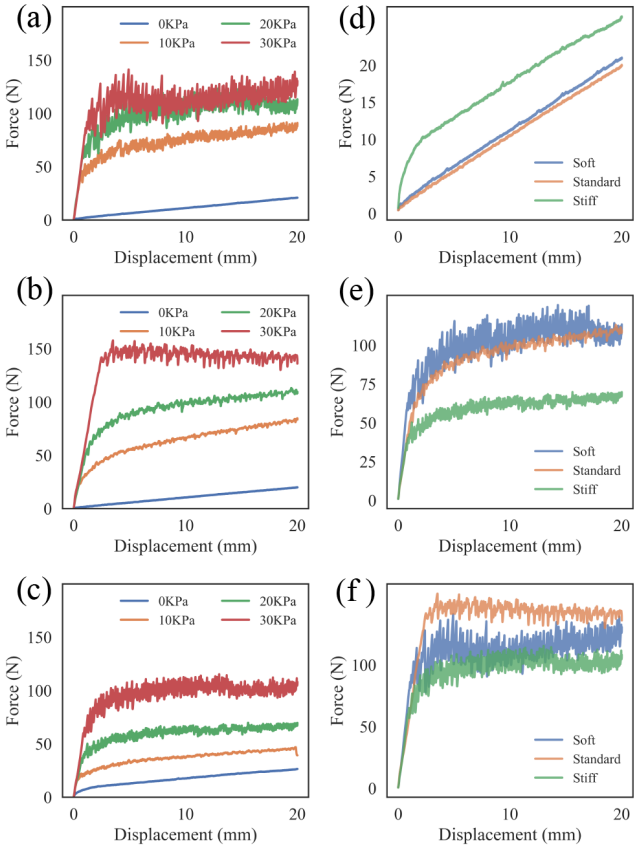

Fig. 4. Variation of stiffness with airbag hardness and inflation pressure. (a) Soft airbag under varying pressure. (b) Standard airbag under varying pressure. (c) Stiff airbag under varying pressure. (d) Comparison of different hardness values at 0 kPa. (e) Comparison of different hardness values at 20 kPa. (f) Comparison of different hardness values at 30 kPa.

Ecoflex™ 00-30(soft), Ecoflex™ 00-50(standard), and TY-866AB(stiff).

Fig. 4 presents the force-displacement curves under the influence of airbags with varying material properties. It can be observed that in the absence of air pressure (0 kPa), different airbag types have minimal impact on the structural stiffness. This behavior occurs because the airbag is fixed only at one end, leaving the remainder unconstrained. During tensile loading, the airbag does not restrict the motion of the structure and therefore contributes little to the overall stiffness.

In Fig. 4.(d), the airbag made of TY-866AB material exhibits a noticeable force increase within the initial 3 mm of displacement. This is attributed to the initial pre-compression state of the stiffer airbag, which possesses inherent elasticity. As the tensile displacement continues, this effect diminishes, and the overall stiffness converges to that of the corrugated spring shell alone. In Fig. 4(e), under low air pressure, the structure with a soft airbag exhibits a rapid increase in stiffness. This behavior occurs because softer airbags expand more easily under minimal pressure, applying uniform compression across the entire overlapping region of the jamming plates. In contrast, airbags made of higher-hardness silicone do not fully expand at low pressure,

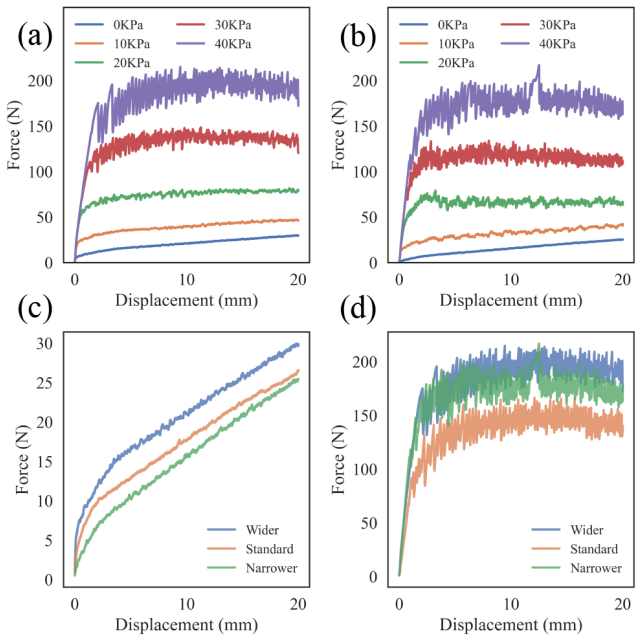

Fig. 5. Tensile behavior of jamming plates with different geometries under varying air pressure. (a) Wider plate under different pressures. (b) Narrower plate under different pressures. (c) Comparison of different plate geometries at 0 kPa. (d) Comparison of different plate geometries at 30 kPa.

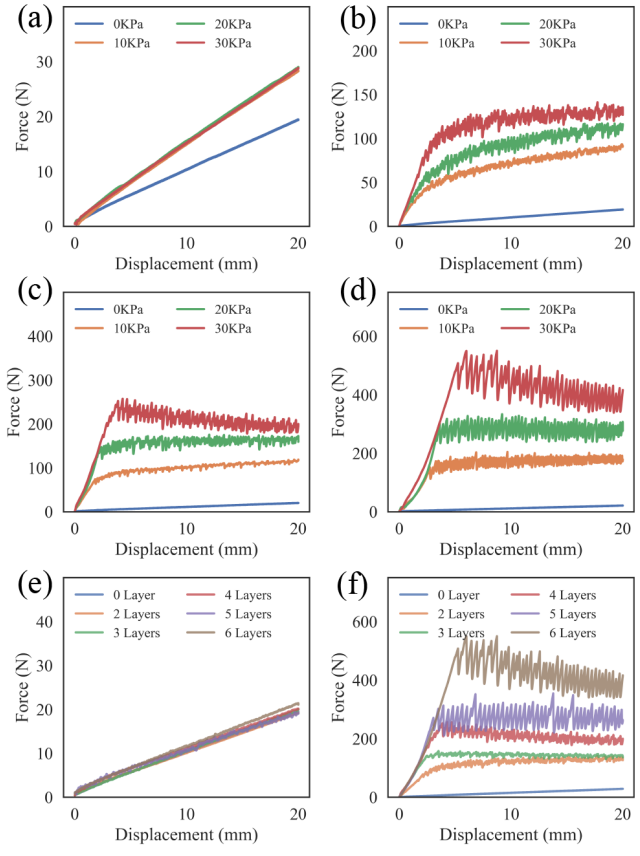

Fig. 6. Influence of layer count on tensile behavior under varied air pressure. (a) 0 layers under different pressures. (b) 2 layers under different pressures. (c) 4 layers under different pressures. (d) 6 layers under different pressures. (e) Comparison of different layer counts at 0 kPa. (f) Comparison of different layer counts at 30 kPa.

resulting in only partial compression and a less pronounced stiffness change. As shown in Fig. 4(f), when the air pressure is further increased, the rate of stiffness growth for the soft airbag structure begins to slow compared to that of the stiff airbag. This is due to the fact that, at higher pressures, the compression area becomes more complete even for stiff airbags, reducing the relative advantage of the soft airbag. Additionally, the load-bearing capacity of the soft airbag is limited, which constrains the overall range of stiffness variation achievable under high pressure conditions.

During tensile testing, repeated force jumps were observed, a phenomenon attributed to cyclic transitions between locking and sliding states within the jamming layers, as described in [31]. The magnitude of these fluctuations is influenced by factors including material properties, tensile rate, and external conditions. Although this effect has limited impact on overall structural performance, the force threshold at which sliding initiates can be defined as $F_{\max}$. By introducing a safety coefficient k, the structure can maintain high stiffness without sliding under an applied external force lower than $kF_{\max}$.

It is observed that the evolution of the force-displacement curves after entering the stick-slip phase varies significantly with changes in air pressure. At high pressure levels, the curves exhibit an overall downward trajectory, a phenomenon that is characterized by (8).

To evaluate the effect of jamming plate shape on structural stiffness, three configurations with varying contact widths—wide, normal, and narrow—were tested using a three-layer assembly under multiple air pressure conditions. As shown in Fig. 5, the tensile tests indicate that while the contact area does influence structural stiffness to some extent, its effect is relatively limited. Variations in plate width result in approximately 20% differences in both stiffness and load capacity. It was also observed that excessively wide jamming plates are prone to flexible deformation (e.g., bending), which can cause mechanical interference and interlayer misalignment during operation. Therefore, a moderate plate width is recommended to ensure structural stability and avoid undesired kinematic interactions.

To evaluate the influence of the number of jamming plates and their structural configuration on stiffness, the quantity of jamming plates per side was varied from 0 to 6 (i.e., 0, 2, 3, 4, 5, and 6 layers), resulting in $2n-1$ contact surfaces for $n$layers. Each configuration was tested under multiple air pressure conditions, and tensile force-displacement curves were recorded to assess the structural stiffness under various jamming states.

Fig. 6 presents the tensile test results. Analysis clearly indicates that the tensile resistance of the structure increases with the number of jamming layers. The six-layer configuration achieved the highest load-bearing capacity, sustaining 500 N without sliding. In Fig. 6(a), it can be observed that in the absence of jamming plates (0 layers), a slight stiffness increase occurs during inflation due to the additional rigidity provided by the airbag. This effect remains consistent across different pressure levels, as the elongation

of the airbag under pressure contributes measurably to the overall stiffness. Since the same airbag was used throughout these experiments, the stiffness enhancement remains stable under various pressure conditions. In structures incorporating jamming plates, both increasing air pressure and adding more layers led to corresponding graded improvements in load capacity and structural stiffness.

Table I summarizes the key experimental results, clearly indicating that both the load capacity and stiffness increase significantly with the number of jamming layers and the air pressure. In contrast, the influence of airbag hardness and jamming plate width is relatively minor.

TABLE I
SUMMARY OF TENSILE TEST RESULTS UNDER VARIOUS DIFFERENT CONDITIONS

30kPa, 3Layers, Stiff Airbag			30kPa, 3Layers			
Shape	Wider	Narrower	*Hardness*	Soft	Standard	Stiff
K_{max}(N/mm)	80.21	64.63	K_{max}(N/mm)	82.81	58.99	60.46
F_{max}(N)	110	92	F_{max}(N)	101	143	90
Standard Airbag, 30kPa						
Layers	0	2	3	4	5	6
K_{max}(N/mm)	**1.41**	36.12	58.85	65.70	91.67	**100.17**
F_{max}(N)	**28**	107	163	249	318	**511**
3Layers , Stiff Airbag						
Pressure(kPa)	0	10	20	30	40	50
K_{max}(N/mm)	**1.25**	55.17	55.56	68.73	77.57	**87.72**
F_{max}(N)	**25**	45	55	90	130	**160**

C. Physical load tests of single-unit and dual-unit robotic arm configurations

To better demonstrate the stiffness adaptability and load capacity of the structure, a series of suspended-load tests were carried out. As shown in Fig. 7(a), the deformation under a 0.5 kg load decreases progressively as air pressure increases from 0 to 30 kPa, with negligible displacement observed at 20 kPa and 30 kPa, indicating a substantial increase in structural stiffness.

A single module cannot support a 1.5 kg end load in the bent state at 0 kPa, but demonstrates the ability to carry this load when sufficient air pressure is applied.Fig. 7(b) displays the structure supporting loads of 0.5 kg, 1.5 kg, and 2 kg under a constant pressure of 30 kPa. Fig. 7(c) compares the deformations under 0.5 kg and 1.5 kg loads in both forward and reverse bending directions at 30 kPa. Significantly larger deformation occurs during reverse bending compared to forward bending or horizontal loading. This behavior can be attributed to the internal airbag's tendency to restore to a straight configuration under pressure. As the bending angle grows, the airbag exerts an increasing restorative force, enhancing structural stiffness in forward bending but providing less resistance in reverse bending.

Fig. 8(a) illustrates the complete dual-unit robotic arm test setup. Three stepper motors, mounted on the base, actuate tendons to control bending and contraction of the arm. The airbags in both units are connected in series via

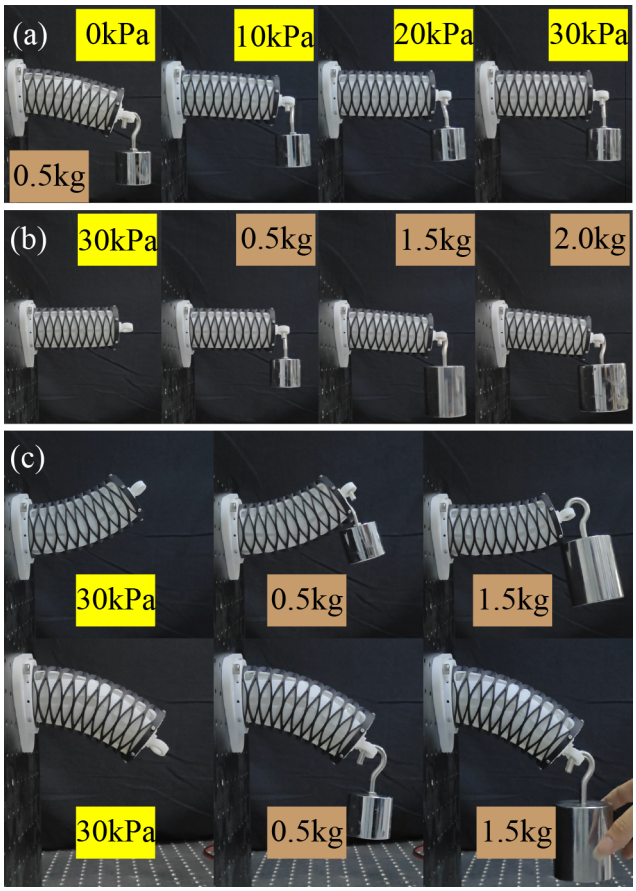

Fig. 7. Load-bearing and bending performance of the structural unit: (a) Suspension of a 0.5 kg weight under varying air pressures. (b) Suspension of different weights under 30 kPa air pressure. (c) Forward and reverse bending deformation with suspended loads of 0.5 kg and 1.5 kg at 30 kPa.

tubing to an external pressure regulator. Fig. 8(b) shows the arm in a partially bent state. Since the three tendons are evenly distributed around the periphery, the arm can achieve omnidirectional bending, with a maximum bending angle of 90°.

Fig. 9(a) demonstrates the load capacity of the integrated arm under different air pressures. As pressure increases, structural stiffness rises and deformation decreases markedly. Fig. 9(b) shows the arm supporting a load at 30 kPa without tendon actuation, indicating self-locking capability through jamming plate engagement under air pressure.

These tests confirm that the structure exhibits a wide range of stiffness adjustability and can adapt to varying task requirements through appropriate pressure regulation.

IV. CONCLUSION AND FUTURE WORK

In this study, we designed and investigated a layer jamming structure integrated within a corrugated spring shell, which enables variable stiffness through positive pneumatic pressure applied to compress the jamming layers. A series of comparative experiments demonstrated that increasing both the number of jamming plates and the air pressure significantly enhances the load-bearing capacity of the structure. The maximum load capacity reached 500 N, with an

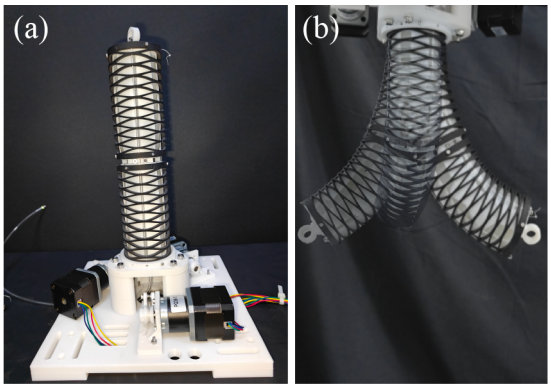

Fig. 8. (a) Dual unit testing structure. (b) Structural Movement Display.

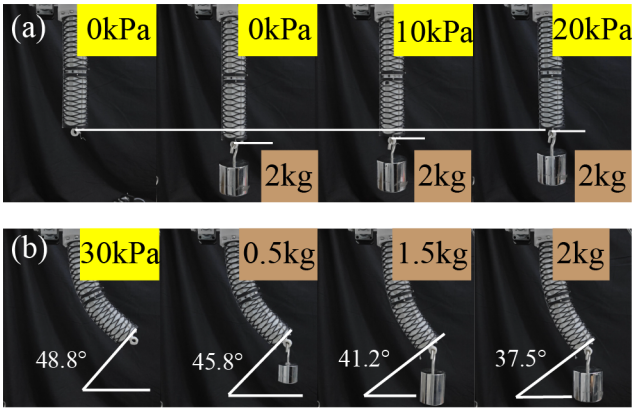

Fig. 9. Load capacity of the dual-unit soft arm under passive conditions (tendons unactuated): (a) Deformation under a 2 kg load at different air pressures. (b) Load-bearing performance in a bent configuration at 30 kPa without tendon support.

equivalent structural stiffness of approximately 100 N/mm, representing an approximately 70-fold increase in stiffness and a 20-fold improvement in load capacity compared to the baseline configuration. Additional findings indicate that softer airbags provide better performance at low pressures, while the geometry of the jamming plates has a relatively minor influence on the variable stiffness behavior.

Subsequent bending load tests on a single unit showed a remarkable improvement in performance: without pressure, the structure could not support a 1.5 kg weight, whereas at 30 kPa it sustained a 2 kg load with negligible deformation. These results confirm that stiffness modulation substantially enhances load capacity even under bending conditions. Further tests were conducted on a two-unit serial arm prototype to evaluate its motion range and load-bearing capability, demonstrating effective passive load support in a self-locked state.

For future work, we plan to optimize the internal structure by concentrating pressure on the overlapping regions of the jamming layers and exploring higher pressure levels to further exploit the advantages of positive-pressure actuation. We also intend to develop a dual-chamber airbag system to enable active elongation of the structure. Additionally, we will incorporate and model an antagonistic variable-stiffness mechanism, with the goal of establishing a unified stiffness model for both jamming and antagonistic principles. Finally, control strategies will be optimized to facilitate adaptive operation of the soft arm across different stiffness regimes.

REFERENCES

[1] J.Zhu et al."Bioinspired multimodal multipose hybrid fingers for wide-range force, compliant, and stable grasping," Soft Rob., Feb. 2023.
[2] F. I. ț Birouaș, I. C. Țarcă, and R. C. Țarcă, "Kinematic model of a new soft-rigid hybrid robotic hand exoskeleton," in Mechanism Design for Robotics, E.-C. Lovasz, M. Ceccarelli, and V. Ciupe, Eds., Cham: Springer Nature Switzerland, 2024, pp. 279–288.
[3] X. Fu, D. Zhang, N. Xu, S. Ren, Y. Chu and X. Zhao, "A Soft–Rigid Coupled Gripper Driven by a Self-Sensing Origami Actuator for Compliant and Robust Grasping," in IEEE/ASME Transactions on Mechatronics.
[4] S. Jiang et al. , "A variable-stiffness continuum manipulators by an SMA-based sheath in minimally invasive surgery," Int. J. Med. Rob. Comput. Assisted Surg. , vol. 16, no. 2, p. e2081, Apr. 2020.
[5] K. Yan et al. , "Towards a wristed percutaneous robot with variable stiffness for pericardiocentesis," IEEE Robot. Autom. Lett. , vol. 6, no. 2, pp. 2993–3000, Apr. 2021.
[6] Y.-J. Kim, S. Cheng, S. Kim, and K. Iagnemma, "A stiffness-adjustable hyperredundant manipulator using a variable neutral-line mechanism for minimally invasive surgery," IEEE Trans. Robot. , vol. 30, no. 2, pp. 382–395, Apr. 2014.
[7] I. A. Seleem, M. A. Naeem, and H. Ishii, "Design and analysis of extensible cable-driven continuum robot with variable stiffness," in 2023 IEEE International Conference on Robotics and Biomimetics (ROBIO) , Dec. 2023, pp. 1–8.
[8] Yigit, C. B. and Boyraz, P.: Design and Modelling of a Cable-Driven Parallel-Series Hybrid Variable Stiffness Joint Mechanism for Robotics, Mech. Sci., 8, 65–77, 2017.
[9] Alok Ranjan Sahoo, Pavan Chakraborty; Development and analysis of a bio-inspired wire-driven variable stiffness double spring based tapered multi-section flexible robot. Industrial Robot 11 February 2022; 49 (2): 187–199.
[10] Zhuang Zhang, Shujie Tang, Weicheng Fan, Yuanhao Xun, Hao Wang, Genliang Chen, Design and analysis of hybrid-driven origami continuum robots with extensible and stiffness-tunable sections, Mechanism and Machine Theory,Volume 169,2022,104607,ISSN 0094-114X.
[11] X. Fu, D. Zhang, L. Mo, K. Li, and X. Zhao, "Design and analysis of soft hybrid-driven manipulator with variable stiffness and multiple motion patterns," in 2024 IEEE International Conference on Robotics and Automation (ICRA) , May 2024, pp. 2979–2985.
[12] J. Liu, X. Wang, S. Liu, J. Yi, X. Wang, and Z. Wang, "Vertebraic soft robotic joint design with twisting and antagonism," IEEE Robot. Autom. Lett. , vol. 7, no. 2, Art. no. 2, Apr. 2022.
[13] Y. Zhang et al. , "Stiffness analysis of a pneumatic soft manipulator based on bending shape prediction," IEEE Access , vol. 8, pp. 82227–82241, 2020.
[14] [1] X. Liu, L. Lin, Z. Song, J. Li, and L. Xu, "A variable stiffness soft robotic hand featuring ball-jointed skeleton coupled with particles," J. Mech. Des., vol. 147, no. 8, Art. no. 83305, Aug. 2025.
[15] L.-J. Gai, J. Huang, and X. Zong, "Stiffness-tunable soft bellows actuators by cross-fiber jamming effect for robust grasping," IEEE/ASME Trans. Mechatronics, vol. 28, no. 5, Art. no. 5, Oct. 2023.
[16] S. Jadhav, M. R. A. Majit, B. Shih, J. P. Schulze, and M. T. Tolley, "Variable stiffness devices using fiber jamming for application in soft robotics and wearable haptics," Soft Rob., Feb. 2022.
[17] J. Kang, S. Lee, and Y.-L. Park, "Soft bending actuator with fiber-jamming variable stiffness and fiber-optic proprioception," IEEE Robot. Autom. Lett., vol. 8, no. 11, pp. 7344–7351, Nov. 2023.
[18] M. S. Moses, M. D. M. Kutzer, H. Ma, and M. Armand, "A continuum manipulator made of interlocking fibers," in 2013 IEEE International Conference on Robotics and Automation, May 2013, pp. 4008–4015.
[19] L. Arleo and M. Cianchetti, "VARISA - a VARIable stiffness soft robotics arm based on inverse pneumatic actuators and differential drive fiber jamming," Mechatronics, vol. 102, p. 103230, Oct. 2024.
[20] Y.-J. Kim, S. Cheng, S. Kim, and K. Iagnemma, "A novel layer jamming mechanism with tunable stiffness capability for minimally invasive surgery," IEEE Trans. Robot., vol. 29, no. 4, pp. 1031–1042, Aug. 2013.

[21] I. Choi, N. Corson, L. Peiros, E. W. Hawkes, S. Keller, and S. Follmer, "A soft, controllable, high force density linear brake utilizing layer jamming," IEEE Robot. Autom. Lett., vol. 3, no. 1, pp. 450–457, Jan. 2018.

[22] F. Xu, K. Ma, X. He, M. Wei, and C. Hu, "Design, analysis, and testing of a variable-stiffness soft grabbing robot coupling particle jamming and layer jamming," Smart Mater. Struct., vol. 33, no. 5, p. 55036, Apr. 2024.

[23] X. Zeng and H.-J. Su, "A high performance pneumatically actuated soft gripper based on layer jamming," J. Mech. Rob., vol. 15, no. 1, p. 14501, Feb. 2023.

[24] Y. Fan, D. Liu, and L. Ye, "A novel continuum robot with stiffness variation capability using layer jamming: design, modeling, and validation," IEEE Access, vol. 10, pp. 130253–130263, 2022.

[25] T. Chen, X. Yang, B. Zhang, J. Li, J. Pan, and Y. Wang, "Scale-inspired programmable robotic structures with concurrent shape morphing and stiffness variation," Sci. Rob., 2024.

[26] J. L. C. Santiago, I. S. Godage, P. Gonthina, and I. D. Walker, "Soft robots and kangaroo tails: modulating compliance in continuum structures through mechanical layer jamming," Soft Rob., vol. 3, no. 2, pp. 54–63, Jun. 2016.

[27] T. Wang, J. Zhang, Y. Li, J. Hong, and M. Y. Wang, "Electrostatic layer jamming variable stiffness for soft robotics," IEEE/ASME Trans. Mechatronics, vol. 24, no. 2, pp. 424–433, Apr. 2019.

[28] P. Li, Y. Zhang, J. Quan, G. Zhang, D. Zhou, and L. Li, "Enhanced deformation resistance and load-bearing capacity in tip-growing robots through scale-inspired layer jamming mechanism," Soft Rob., p. soro.2024.147, Jun. 2025.

[29] E. H. Skorina and C. D. Onal, "Soft hybrid wave spring actuators," Adv. Intell. Syst., vol. 2, no. 1, p. 1900097, 2020.

[30] J. M. Salgueiro and J. C. P. Reis, "Towards a highly integrated 3D printed soft continuum manipulator," in 2021 7th International Conference on Automation, Robotics and Applications (ICARA), Feb. 2021, pp. 163–167.

[31] I. Choi, N. Corson, L. Peiros, E. W. Hawkes, S. Keller, and S. Follmer, "A soft, controllable, high force density linear brake utilizing layer jamming," IEEE Robot. Autom. Lett., vol. 3, no. 1, pp. 450–457, Jan. 2018.